Journal of Engineering Mathematics **30:** 151–168, 1996.
© 1996 *Kluwer Academic Publishers. Printed in the Netherlands.*

Ciliary propulsion, chaotic filtration and a 'blinking' stokeslet

J.R. BLAKE and S.R. OTTO
School of Mathematics and Statistics, The University of Birmingham, Edgbaston, Birmingham B15 2TT, United Kingdom

Received 3 May 1995

Abstract.
The paper discusses the fundamental singularity of Stokes flow (the *stokeslet*) in the context of applications to locomotion and feeding currents in micro-organisms. The image system for a *stokeslet* in a rigid plane boundary may be derived from Lorentz's mirror image technique [1] or by an appropriate limit of Oseen's solution for a sphere near a plane boundary [2]. An alternative derivation using Fourier transform methods [3] leads to an immediate physical interpretation of the image system in terms of a *stokeslet* and its multipole derivatives. The schematic illustration of a *stokeslet* and its image system in a plane boundary are exploited to explain the fluid dynamical principles of ciliary propulsion. For a point force oriented normal to the plane boundary, the resulting axisymmetric motion leads to a Stokes stream function representation which illustrates the toroidal eddy structure of the flow field. A similar eddy structure is also obtained for the two-dimensional system, although in this case, the toroidal structure is replaced by two eddies. This closed streamline model is developed to model chaotic filtration through the concept of a 'blinking *stokeslet*', a *stokeslet* alternating its vertical position according to a specific protocol. The resulting behaviour is illustrated *via* Poincaré sections, particle dispersion and length of particle path tracings. Sessile micro-organisms may exploit a similar process so they can filter as large a volume of liquid as possible in search of food and nutrients.

1. Introduction

The motivation for this paper in the Lorentz issue comes from the field of Biological Fluid Mechanics or, more specifically, from the locomotion and feeding mechanisms of micro-organisms. In micro-organisms, propulsion or feeding currents are normally due to the beating of flagella or cilia (see *e.g.* Gray [4], Sleigh [5]). Flagella propagate a symmetric bending wave along the organelle as occurs in spermatozoa and flagella. The other form of propulsion consists of a dense covering of beating cilia over the external surface of the organism which we now discuss at some length.

A cilium is a small hair-like appendage attached to the surface of the organism. The beat of a single cilium can be separated into two distinct phases, one phase being the fast effective stroke when the cilium drives the fluid in the desired direction, and the other phase being the recovery stroke when the cilium seeks to minimise its influence on fluid motion. The classical case of an effective beat is when the cilium beats near rigidly in its effective stroke, but retreats limply near the organism's surface during the recovery stroke. Many small microscopic organisms are propelled by high concentrations of cilia in rows along and across the surface of the organism. The movements of adjacent cilia in one direction are out of phase, this phenomenon being called metachronism (cf. synchronisation). Thus, viewed from above (or side on), the motion of all cilia appears as a wave passing over the organism. This is often compared to the waving motion observed in a cornfield when a wind is blowing over it. Well-known organisms include the two protozoa *Opalina* and *Paramecium* and the ctenophores ('comb bearers').

Cilia are involved in functions other than those of locomotion, some of these being cleansing, feeding, excretion and reproduction. They exist in nearly all phyla of the animal kingdom. In particular we consider possible models for the generation of feeding currents by sessile organisms (*e.g. Vorticella, Stentor*) in the latter sections of this paper. Examples of a ciliary beat cycle, a wave of cilia and sessile feeding organisms are illustrated in Fig. 1. In these examples the kinematics and dynamics involve the application of a force on a fluid immediately adjacent to a stationary no-slip boundary.

Micro-organisms are very small and move with low velocities so that the Reynolds number is very small. Thus the propulsion of micro-organisms and the generation of feeding currents is dominated by viscous forces rather than the inertial effect we associate with the propulsion of larger and faster objects such as fish, ships and aeroplanes.

Functionally, cilia move in fluid parallel to the micro-organism's exterior surface. Since we are discussing the motion of cilia in the vicinity of the organism's surface it proves essential for us to know the Green's function of the Stokes flow equations in the presence of a stationary plane boundary. Because cilia are long slender bodies we can approximate the velocity and pressure field by a distribution of these singularities along the centreline of the slender body. Thus the basic problem in terms of the equations of motion is,

$$\left.\begin{aligned} \nabla p &= \mu \nabla^2 \mathbf{u} + \mathbf{F}\delta(\mathbf{x}-\mathbf{y}) \\ \nabla \cdot \mathbf{u} &= 0 \end{aligned}\right\}, \tag{1}$$

where $\mathbf{u} = \mathbf{0}$ on $x_3 = 0$. Here $\mathbf{u}$ is the velocity vector, p the pressure, μ the dynamic viscosity, $\mathbf{F}$ the force while $\delta(\mathbf{x}-\mathbf{y})$ is the Dirac delta function.

A solution to this problem can be obtained by using the method derived by Lorentz [1] from a reciprocal theorem. This Green's function can also be obtained from the approximate solution in Oseen [2] for the motion of a sphere in the vicinity of a plane boundary. Blake [3] used a much more direct method *via* Fourier transforms which yields the exact form of

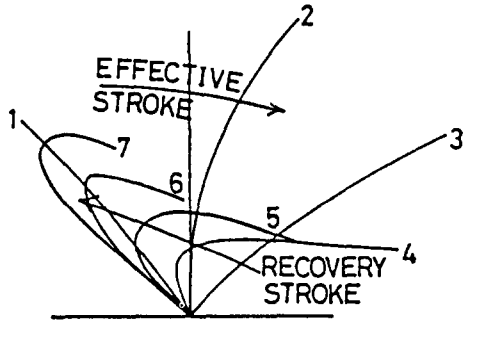

(a)

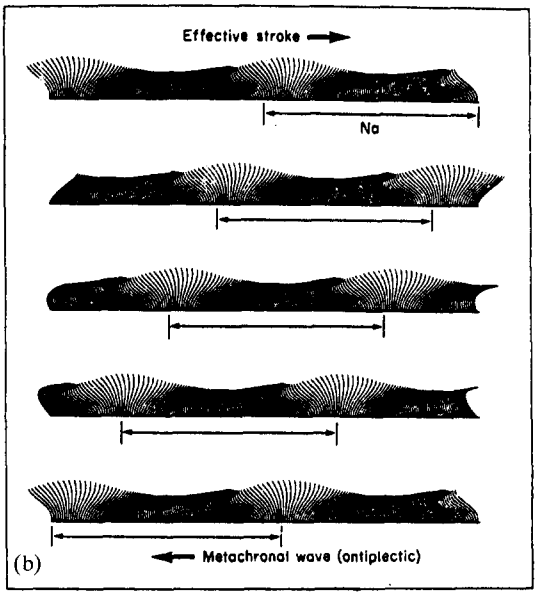

(b)

Fig. 1. (a) An example of a ciliary beat cycle showing the effective and recovery strokes. (b) Wave of cilia showing their coordination in antiplectic metachronism [6]. (c) Sessile organisms *Vorticella* [5] and (d) *Stentor* illustrating the stalk shortening and currents [5].

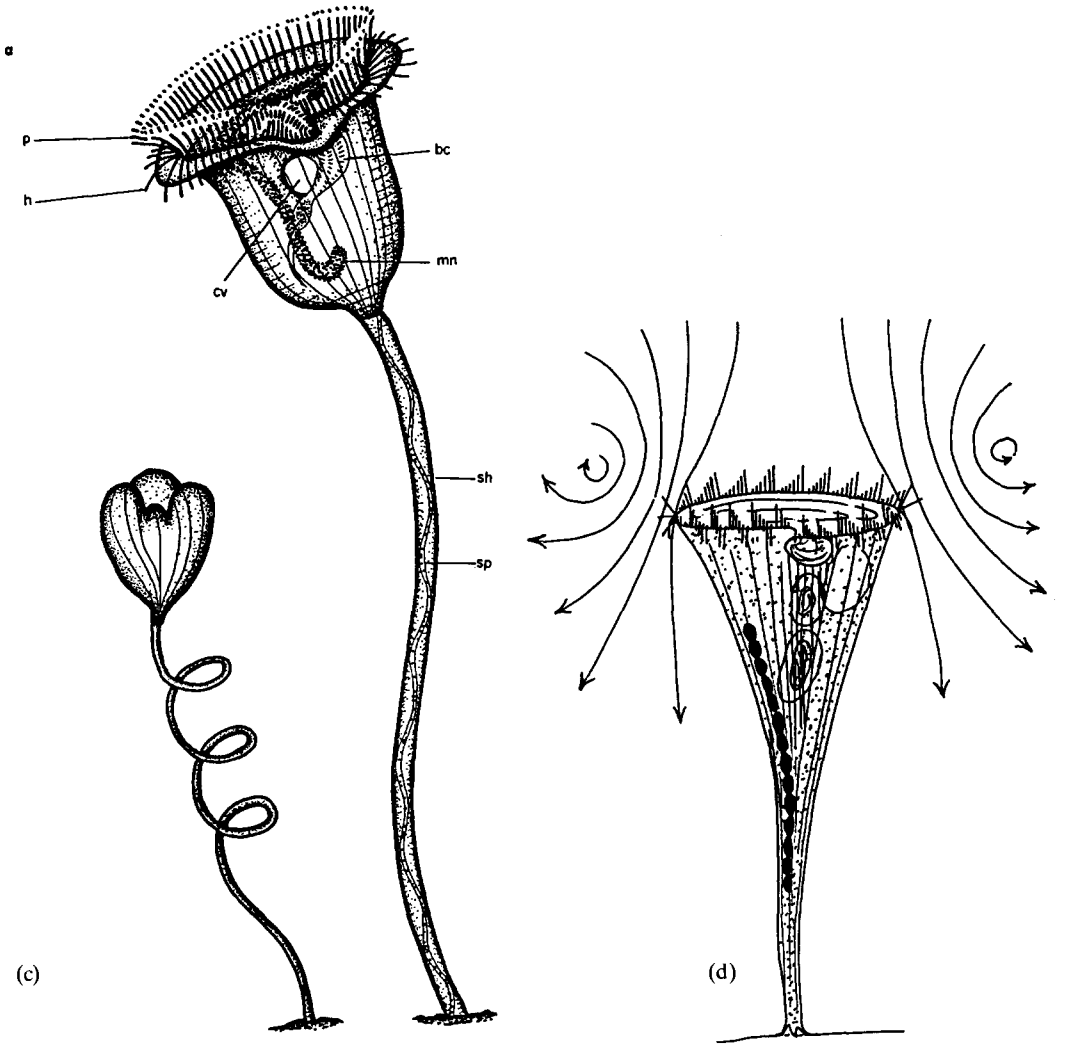

Fig. 1. contd.

the image system. The resulting far-fields obtained for the Green's function prove to be of considerable interest with regard to our understanding of ciliary propulsion and filter feeding. This aspect is discussed in greater depth in a later section. Blake and Chwang [7] extended this approach further to other singularities near a rigid boundary.

2. Some history

2.1. Lorentz's mirror image technique

Lorentz [1] developed a simple technique to satisfy the no-slip condition on a plane boundary in Stokes flow from the reciprocal theorem

$$\int_S \sigma' \cdot \mathbf{v}'' \, \mathrm{d}\mathbf{S} = \int_S \sigma'' \cdot \mathbf{v}' \, \mathrm{d}\mathbf{S}, \tag{2}$$

where $(\mathbf{v}', \sigma')$ and $(\mathbf{v}'', \sigma'')$ are the velocity and stress fields corresponding to any two motions in the same fluid. He derived a formula to obtain the image motion which, together with

the original movement in an unbounded fluid, will satisfy the no-slip condition on the plane $x_3 = 0$.

As we are only interested in the fundamental singularity of the Stokes' flow equations, we will consider the velocity and pressure fields due to a point force (*'stokeslet'*) at the point (y_1, y_2, h) $(h > 0)$. These are,

$$\left.\begin{aligned} v_i' &= \frac{F_j}{8\pi\mu}\left(\frac{\delta_{ij}}{r} + \frac{r_i r_j}{r^3}\right), \\ p' &= \frac{F_j r_j}{4\pi r^3}, \end{aligned}\right\} \tag{3}$$

where $r = [(x_1 - y_1)^2 + (x_2 - y_2)^2 + (x_3 - h)^2]^{\frac{1}{2}}$ with the component r_i being obvious from this definition.

The reflected motion in the negative half plane for the unbounded fluid $(x_3 < 0)$ is,

$$\left.\begin{aligned} u_i &= \frac{F_j}{8\pi\mu}(\delta_{k\alpha}\delta_{\alpha j} - \delta_{j3}\delta_{k3})\left(\frac{\delta_{ik}}{R} + \frac{R_i R_k}{R^3}\right) \\ p &= \frac{F_j}{4\pi}(\delta_{k\alpha}\delta_{\alpha j} - \delta_{j3}\delta_{k3})\frac{R_k}{R^3}, \quad \alpha = 1,2 \end{aligned}\right\}, \tag{4}$$

where $R = [(x_1 - y_1)^2 + (x_2 - y_2)^2 + (x_3 + h)^2]^{\frac{1}{2}}$ with the components R_i being immediately apparent from this definition.

The image system required by Lorentz to satisfy the no-slip conditions is given by,

$$\left.\begin{aligned} v_i'' &= (-\delta_{i\alpha}\delta_{\alpha k} + \delta_{i3}\delta_{k3})u_k - 2x_3\frac{\partial u_3}{\partial x_i} + \frac{x_3^2}{\mu}\frac{\partial p}{\partial x_i} \\ p'' &= p + 2x_3\frac{\partial p}{\partial x_3} - 4\mu\frac{\partial u_3}{\partial x_3} \end{aligned}\right\}. \tag{5}$$

Substitution of (4) in (5) yields,

$$\left.\begin{aligned} v_i'' &= \frac{F_j}{8\pi\mu}\left[-\left(\frac{\delta_{ij}}{R} + \frac{R_i R_j}{R^3}\right) + 2h(\delta_{j\alpha}\delta_{\alpha k} - \delta_{j3}\delta_{3k})\frac{\partial}{\partial R_k}\left\{\frac{hR_i}{R^3} - \left(\frac{\delta_{i3}}{R} + \frac{R_i R_3}{R^3}\right)\right\}\right], \\ p'' &= \frac{F_j}{4\pi}\left[\frac{-R_j}{R^3} - 2h(\delta_{j\alpha}\delta_{\alpha k} - \delta_{j3}\delta_{3k})\frac{\partial\,(R_3/R^3)}{\partial R_k}\right]. \end{aligned}\right\} \tag{6}$$

The total velocity and pressure field (i.e. Green's function) for a *stokeslet* near a no-slip plane boundary is thus:

$$\left.\begin{aligned} \mathbf{u} &= \mathbf{v}' + \mathbf{v}'', \\ p &= p' + p''. \end{aligned}\right\} \tag{7}$$

2.2. Oseen's solution for a sphere in Stokes flow near a plane wall

In his book, Oseen [2] obtains an approximate solution for the motion of a sphere near a stationary plane wall in Stokes flow. The solution obtained is the initial unbounded motion

$$\left.\begin{aligned} u_j &= \frac{3}{2}aU_j - \frac{a}{4}U_k\frac{\partial^2}{\partial x_j \partial x_k}\left(3r + \frac{a^2}{r}\right), \\ p &= -\frac{3}{2}a\mu U_k\frac{\partial(1/r)}{\partial x_k} \end{aligned}\right\} \tag{8}$$

and the image motion

$$
\begin{aligned}
u^*_\alpha &= -\frac{3}{2}\frac{a}{R}U_\alpha + \frac{a}{4}\sum_{\beta=1,2} U_\beta \frac{\partial^2}{\partial x_\alpha \partial x_\beta}\left(3R + \frac{a^2}{R} + \frac{6hx_3}{R} + 2a^2 x_3 \frac{\partial(1/R)}{\partial x_3}\right) \\
&\quad + \frac{a}{4}U_3 \frac{\partial^2}{\partial x_\alpha \partial x_3}\left(3R + \frac{a^2}{R} - \frac{6hx_3}{R} - 2a^2 x_3 \frac{\partial(1/R)}{\partial x_3}\right), \alpha = 1,2, \\
u^*_3 &= -\frac{9}{2}\frac{a}{R}U_3 - \frac{a}{4}\sum_{\beta=1,2} U_\beta \frac{\partial^2}{\partial x_3 \partial x_\beta}\left(\frac{3(h-x_3)}{R} + a^2 \frac{\partial(1/R)}{\partial x_3}\right) \\
&\quad + \frac{a}{4}U_3 \frac{\partial^2}{\partial x_3^2}\left(15R + \frac{5a^2}{R} - \frac{6hx_3}{R} - 2a^2 x_3 \frac{\partial(1/R)}{\partial x_3} - 3aU_3 x_3 \frac{\partial(1/R)}{\partial x_3}\right).
\end{aligned} \tag{9}
$$

and

$$
\begin{aligned}
p^* &= \tfrac{1}{2}\mu a \sum_{\beta=1,2} U_\beta \frac{\partial}{\partial x_\beta}\left(\frac{3}{R} + 6h\frac{\partial(1/R)}{\partial x_3} + 2a^2 \frac{\partial^2\left(\frac{1}{R}\right)}{\partial x_3^2}\right) \\
&\quad + \frac{1}{2}\mu a U_3 \frac{\partial}{\partial x_3}\left(\frac{3}{R} - 6h\frac{\partial(1/R)}{\partial x_3} - 2a^2 \frac{\partial^2(1/R)}{\partial x_3^2}\right).
\end{aligned}
$$

The total velocity field is again obtained by adding. If we apply the usual limiting process to these equations of

$$
\left.
\begin{aligned}
&\lim_{a\to 0} \frac{3}{4} a U_j = \frac{F_j}{8\pi\mu} \\
&\lim_{a\to 0} a^n U_j = 0; \quad n > 1
\end{aligned}
\right\}, \tag{10}
$$

we obtain the Green's function defined in (7).

2.3. Image system singularity diagram and far-field

Clearly for $r \ll h$, the solution in the near field around the *stokeslet* is that of an isolated *stokeslet* in an infinite viscous fluid. However, the outer field is considerably modified by the presence of the no-slip plane boundary.

To assist with the description of the image system and the singularity diagram, we introduce the concept of a stokes-doublet. Following Batchelor [8], we define a stokes-doublet with tensorial strength D_{jk} as follows:

$$
\begin{aligned}
u'_i &= \frac{D_{jk}}{8\pi\mu}\left[\left\{-\frac{r_i\delta_{jk}}{r^3} + \frac{3r_i r_j r_k}{r^5}\right\} + \left\{\frac{r_k\delta_{ij} - r_j\delta_{ik}}{r^3}\right\}\right], \\
p' &= \frac{D_{jk}}{4\pi}\left(\frac{3r_j r_k}{r^5}\right),
\end{aligned} \tag{11}
$$

where u' is the velocity vector and p' the pressure associated with the stokes-doublet.

This tensorial representation D_{jk} for a stokes-doublet may be interpreted as the negative value of the gradient in the k-direction of a *stokeslet* oriented in the j-direction. The first set of bracketed terms in (11) are symmetric, whereas the second bracket is antisymmetric, which Batchelor [8] calls a stresslet and a couplet respectively (the couplet is sometimes also called

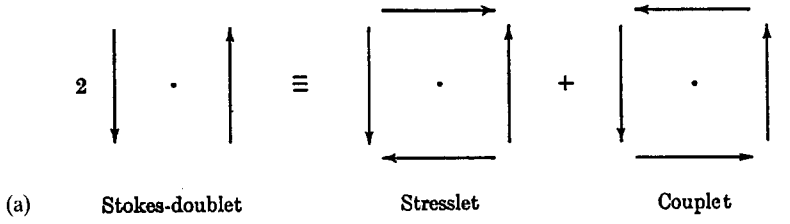

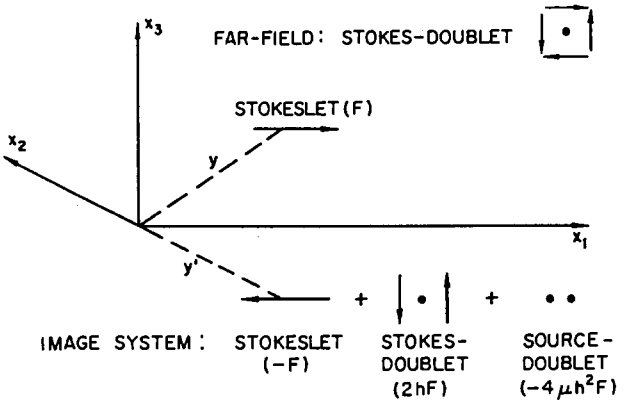

(b)

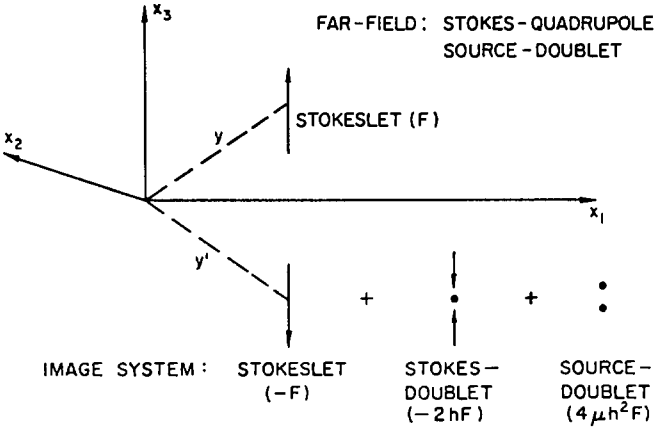

Fig. 2. (a) Stokes doublet decomposition into a stresslet and a couplet. Schematic illustration of the image system for a *stokeslet* (b) parallel and (c) normal to a stationary plane boundary.

the rotlet — see Blake and Chwang [7]). Fig. 2(a) shows the decomposition of a stokes-doublet into a stresslet and a couplet.

The above definition of a stokes-doublet and its singularity decomposition now allows us to illustrate the image systems (Blake [3]) for (i) a *stokeslet* parallel to the plane boundary (Fig. 2(b)) and (ii) a *stokeslet* normal to the plane boundary (Fig. 2(c)). For a *stokeslet* parallel to the boundary the image system at the image point consists of

(i) a *stokeslet* of equal magnitude and opposite sign,

(ii) a stokes-doublet of strength $2h$ of the strength of the *stokeslet*, and

(iii) a source doublet of strength $2h^2$ of the strength of the *stokeslet*.

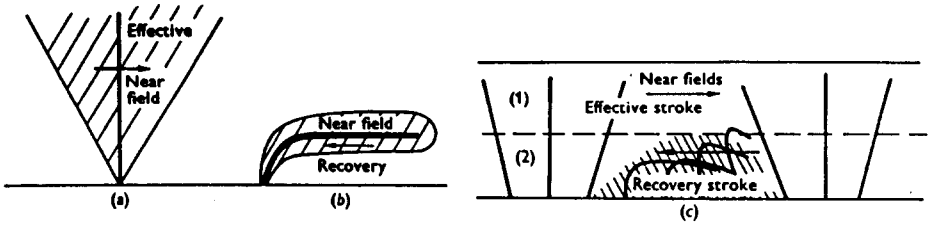

Fig. 3. (a) The *stokeslet* near field during the effective stroke of a cilium; (b) *stokeslet* field during recovery stroke; and (c) the relative near field in a wave of beating cilia. In the upper layer (1) the fluid is influenced primarily by the effective stroke whereas in the lower layer (2), the fluid may be equally influenced by both the effective and recovery strokes.

The stokes-doublet consists of equal and opposite *stokeslets* oriented in the normal (x_3) direction to the plane boundary and with their displacement in the x_1 (or x_2) direction which in the tensorial notation is represented by D_{31} (or D_{32}). Similarly, the source-doublet has displacement axis in the x_1-direction. The stokes-doublet in this case is of magnitude $D_{31} = 2hF_1$, which is equal in strength in the far-field to the combined influence of the initial and image *stokeslets* ($D_{13} = 2hF_1$). Thus in the far-field the antisymmetric component of D_{31} and D_{13} cancel leaving only the symmetric stresslet term. Therefore the far-field asymptote is as follows,

$$u_i \sim \frac{F_\alpha}{8\pi\mu}\left[\frac{6h^2x_3^2\delta_{i\alpha}}{|x|^5} + \frac{12hx_ix_\alpha x_3}{|x|^5}\right] \quad \alpha = 1,2, \quad i = 1,2,3. \tag{12}$$

The alternative orientation for the initial *stokeslet* is in the normal direction to the plane boundary. The image systems consists of

(i) a negative *stokeslet* of equal magnitude,

(ii) a stokes-doublet of strength $(-2hF_3)$, and

(iii) a source-doublet of strength $(2h^2F_3)$.

The stokes-doublet in this case consists of two *stokeslets* equal in magnitude, opposite in sign, oriented in the normal direction yielding only a symmetric stresslet field but with strength $(-2hF_3)$. This exactly counterbalances the *stokeslet* and its image in the far-field $(2hF_3)$ leading to a stokes-quadrupole far-field. However the source-doublet is also a degenerate stokes quadrupole, thus the far-field in this case is of stokes-quadrupole and thence a higher rate of decay $O(1/r^3)$ than the stresslet $O(1/r^2)$ far-field of the case of a *stokeslet* parallel to the plane boundary

$$u_i \sim \frac{F_3}{8\pi\mu}\left[\frac{-6h^2x_3^2}{|x|^5}\delta_{i3} - \frac{12h^2x_ix_3}{|x|^5} + \frac{30h^2x_ix_3^3}{|x|^7}\right]. \tag{13}$$

2.4. Interpretation in a biological context

A physical interpretation of the movement of a cilium in terms of near and far-field influences is illustrated in Fig. 3. We can approximate the region around the force singularity, which has a *stokeslet* $O(1/r)$ velocity field by a sphere of radius $\frac{1}{2}H$. This means that during the effective stroke the cilium influences a relatively large volume of fluid with its *stokeslet* field in comparison to its movement in the recovery stroke when only the region in the close proximity

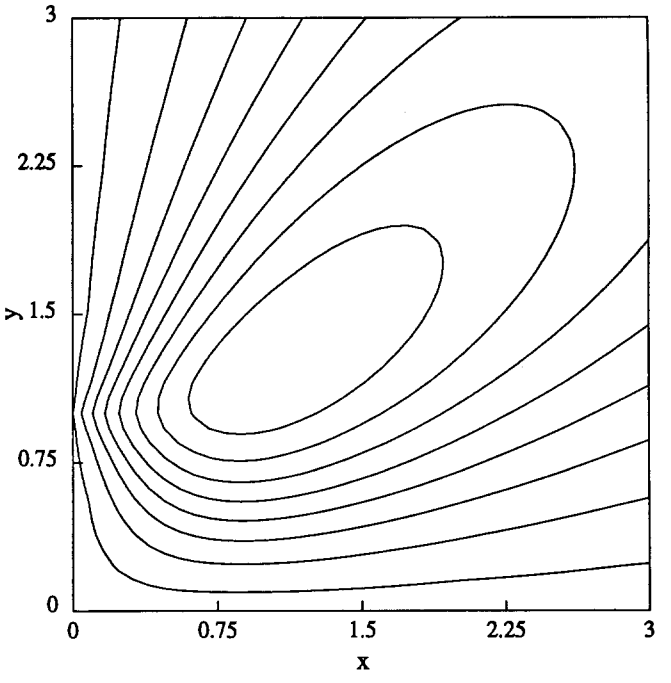

Fig. 4. Streamlines in axisymmetric flow for a point force normal to the stationary no-slip boundary.

of the cilium is influenced by the near-field. Furthermore, one can extend this to a row of cilia in different stages of their beat. The *stokeslet* region influenced by the effective beat consists of the upper half of the ciliary sublayer, while only the lower part feels the recovery stroke. Thus one might anticipate the oscillatory component of the velocity to be small in relation to the mean flow in the upper half of the ciliary sublayer. Conversely, the oscillatory component can be quite large in comparison to the mean flow in the lower part of the sublayer.

Further contributing features to the large effective stroke *stokeslet* region is that the force is larger during the effective stroke. This is due to two factors — one being the larger relative velocities of the effective stroke, the other being due to the fact that a slender body exerts nearly twice the force (for a given velocity) if it moves in a normal direction as against a tangential one.

Experimentally, it is observed (Sleigh and Aiello [9]) that the oscillatory component is small in the uppermost part of the sublayer, but further experimental work needs to be carried out in the lower regions of the cilia sublayer.

2.5. STREAMLINES

(a) **Axisymmetric**

In the case of a *stokeslet* oriented normal to the plane no-slip boundary, the flow field may be represented in terms of a Stokes stream function $\psi(r, z)$, defined in terms of the velocities as follows

$$u_z = \frac{1}{r}\frac{\partial \psi}{\partial r}, \quad u_r = -\frac{1}{r}\frac{\partial \psi}{\partial z}, \tag{14}$$

where r is the radial component and z the vertical one. The stream function obtained by integrating (7) is,

$$\psi(r,z) = \frac{F_3}{8\pi\mu}\left[\frac{r^2}{(r^2+(z-h)^2)^{\frac{1}{2}}} - \frac{r^2}{(r^2+(z+h)^2)^{\frac{1}{2}}} - \frac{2hr^2z}{(r^2+(z+h)^2)^{\frac{3}{2}}}\right]. \quad (15)$$

The resulting streamlines are shown in Fig. 4 where the maximum value of $8\pi\mu\psi/F_3$ is 0.397 when $h = 1$. The interesting feature is the generation of a large toroidal eddy. Aderogba and Blake [10] showed that an eddy will also exist if the no-slip boundary is replaced by a two-fluid interface but not for a stress-free surface.

(b) **Two-dimensional** *stokeslet*

In an analogous way, the equivalent two-dimensional stream function equation yields (Liron and Blake [11])

$$\psi(x,y) = \frac{F}{8\pi\mu}x\left[\frac{1}{2}\log\left\{\frac{x^2+(y+h)^2}{x^2+(y-h)^2}\right\} - \frac{2hy}{x^2+(y+h)^2}\right], \quad (16)$$

where F is directed in the increasing y (vertical) direction with the no-slip boundary given by $y = 0$. The velocity of components is given by,

$$u = \frac{\partial\psi}{\partial y}, \quad v = -\frac{\partial\psi}{\partial x}, \quad (17)$$

where u and v are respectively the velocities in the x and y-directions. However, in the two-dimensional case, two closed eddies (see later in Fig. 6(a)) will be obtained instead of the single toroidal eddy of the previous axisymmetric example.

The stream function equation in (16) will form the basis of the illustrative study of chaotic filtration and dispersion which will form the remainder of this paper. The axisymmetric study may also be developed along exactly the same lines.

3. Modern context

The motivation for this study arises from the feeding currents generated by sessile organisms which are attached to a rigid substrate by a lengthy stalk. The two examples of *Vorticella* and *Stentor* are illustrated in Fig. 1(c) and (d) respectively. Higdon [12] developed a model for the feeding current due to a flagellum, showing the single large toroidal eddy that is developed. This single eddy is not a satisfactory pattern to filter all the water in the near vicinity of the organism because the streamlines are closed and thus will only filter a small fraction of the available nearby volume of fluid. We postulate that the organism alters the length of its stalk periodically, thus yielding a chaotic filtration behaviour for the surrounding liquid leading to all particles in a given volume passing through the 'capture net' in a given time. In the next sections we analyse this hypothesis by considering the 'inverse' problem of particle dispersion through diagnostic tools such as Poincaré sections, the dispersion of a 'blob' of particles and the 'length' around these dispersed particles in an effort to develop some understanding on the potential optimal behaviour of the organism to maximise its feed capture.

4. 'Blinking' stokeslet

The proposed model is based on the concept of a 'blinking *stokeslet*' (after the blinking vortex of Aref [13]) which assumes that a downward oriented point force periodically alters its height above the stationary no-slip boundary; thus, in some way, replicating the motion of the organism.

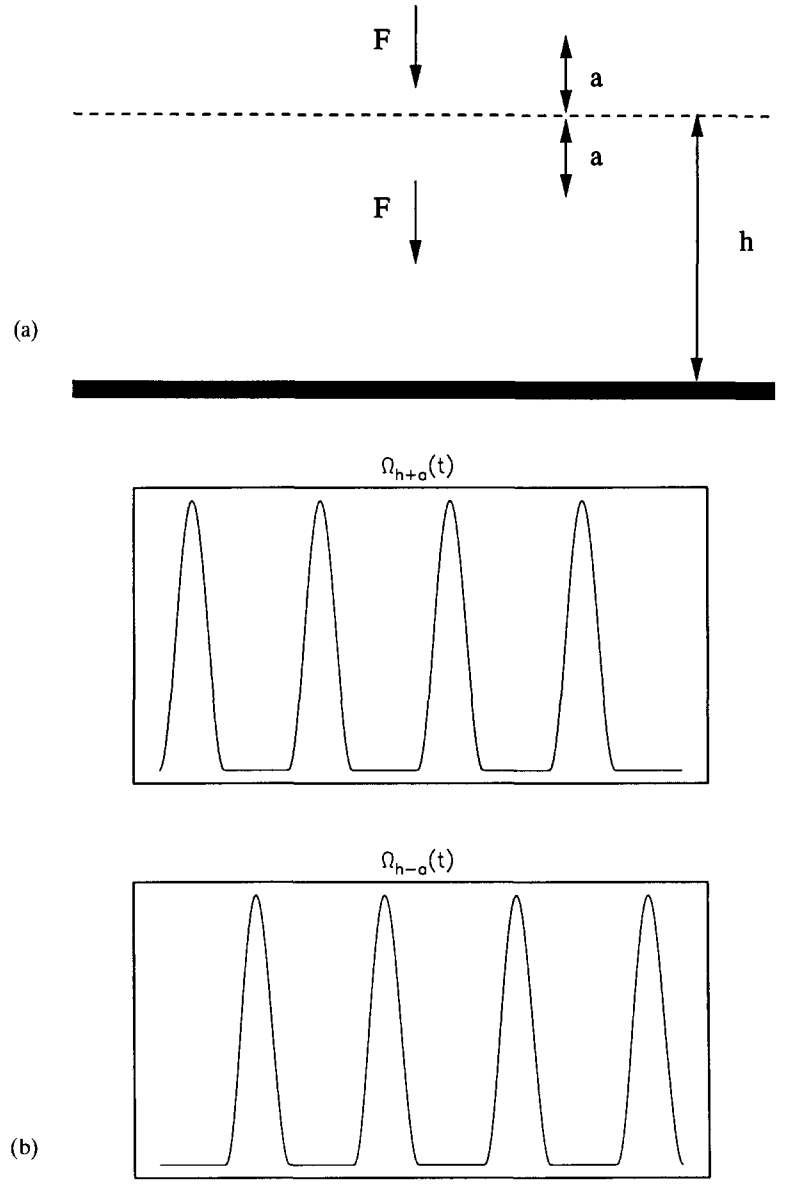

Fig. 5. (a) The geometric configuration for two *stokeslets*. (b) The switching protocol of Eq. (20).

The geometric configuration for the blinking *stokeslet* is illustrated in Fig. 5(a). The downward pointing *stokeslet* changes location every T time units. We shall restrict ourselves to considering constant T, that is the time spent 'with' each *stokeslet* is the same and remains constant. This leads to an overall period for the switching τ, with

$$\tau = 2T. \tag{18}$$

We now suppose that the *stokeslet* is alternatively located at $y = h + a$ and $y = h - a$. Each *stokeslet* has a stream function associated with it ($\psi_{h\pm a}$ at $y = h \pm a$) and the question of how one switches between these needs to be answered. In general we can suppose that

$$\psi(x, y) = \Omega_{h+a}(t)\psi_{h+a}(x, y) + \Omega_{h-a}(t)\psi_{h-a}(x, y).$$

The forms of $\Omega_{h\pm a}(t)$ that we exploit are taken from Aref [13] and Aref & Balachandar [14], in which chaotic advection was considered. In the former article stirring via an agitator was considered, this was modelled via a point vortex (together with its image). The location of the agitator was moved using step functions. The corresponding switching protocol here may be written

$$\Omega_{h+a}(t) = \begin{cases} 1 & \text{for} \quad 2nT < t < (2n+1)T \\ 0 & \text{for} \quad (2n+1)T < t < 2(n+1)T \end{cases} \tag{19a}$$

and

$$\Omega_{h-a}(t) = \begin{cases} 0 & \text{for} \quad 2nT < t < (2n+1)T \\ 1 & \text{for} \quad (2n+1)T < t < 2(n+1)T \end{cases}, \tag{19b}$$

where n is any positive integer.

The second paper considered the flow between two cylinders (non–concentric) in which the angular velocity of the cylinders was turned on and off. More sophisticated protocols were introduced, one of which may be written

$$\Omega_{h\pm a}(t) = 2\Omega^{(0)}_{h\pm a} \sin\left(\frac{t\pi}{\tau}\right)\left(\sin\left(\frac{t\pi}{\tau}\right) \pm \left|\sin\left(\frac{t\pi}{\tau}\right)\right|\right). \tag{20}$$

The advantage of this second technique is that the switching is now differentiable at the switching point. The average strength over the period is given by $\Omega^{(0)}_{h\pm a}$. It is found that the choice of protocol has very little effect on the results, so we will present the results obtained by using the latter, that is (20). In Fig. 5(b) we show four complete periods of the switching for the functions $\Omega_{h\pm a}(t)$.

We can now chose h as a representative length scale ($x = hX$, $y = hY$) and T as a characteristic time scale ($t = T\tilde{t}$). This leads to the following dimensionless parameters

$$\alpha = \frac{FT}{4\mu h}, \qquad \epsilon = \frac{a}{h} \quad (0 < \epsilon < 1).$$

The problem specification now becomes

$$\Psi_{1\pm\epsilon}(X,Y) = \alpha X\left(\frac{1}{2}\log\left(\frac{X^2+(Y+(1\pm\epsilon))^2}{X^2+(Y-(1\pm\epsilon))^2}\right) - \frac{2(1\pm\epsilon)Y}{X^2+(Y+(1\pm\epsilon))^2}\right),$$

with

$$\frac{\mathrm{d}X}{\mathrm{d}\tilde{t}} = \frac{\partial\Psi}{\partial Y}(X,Y) \quad \text{and} \quad \frac{\mathrm{d}Y}{\mathrm{d}\tilde{t}} = -\frac{\partial\Psi}{\partial X}(X,Y). \tag{21}$$

Let us suppose that we consider N particles located at (X^0_n, Y^0_n) for $n = 1 \ldots N$ subject to (21), where $X_n(t=0) = X^0_n$ and $Y_n(t=0) = Y^0_n$. These equations now constitute a Hamiltonian system. We shall discuss our results involving a varying τ (this has a direct correspondence with the *stokeslet* strength α).

In order to integrate these equations we used a fourth order symplectic technique as described in De Frutos & Sanz–Serna [15]. This uses an optimised implicit method rather than, for example, a standard explicit method (fourth order Runge-Kutta). We choose to present our results as Poincaré sections, which are stroboscopic images. The initial array of particles is progressed forward and a dot is drawn when $t = n\tau$. The section is used purely as

(a)

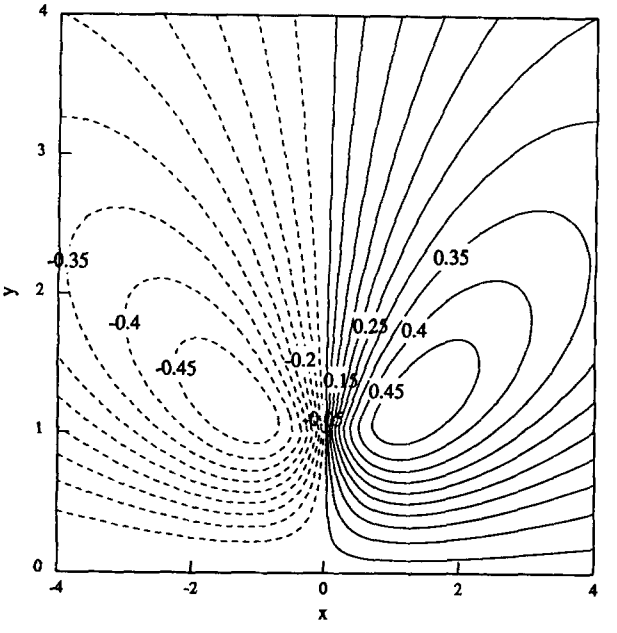

(b)

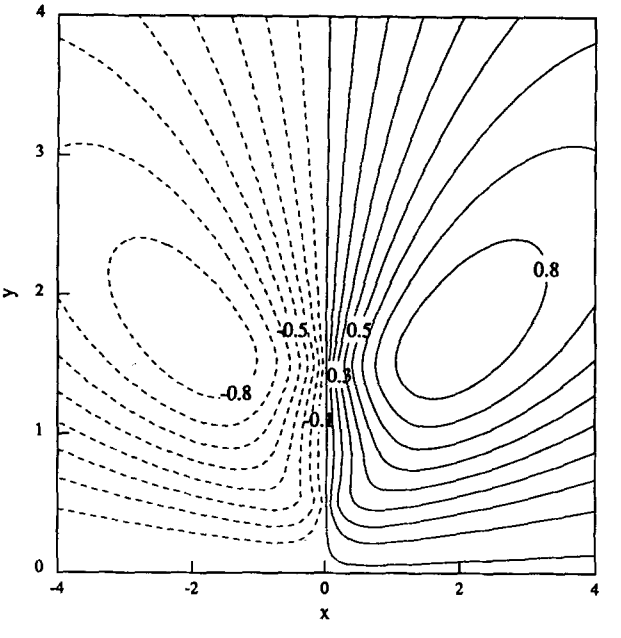

Fig. 6. The streamlines for (a) $\epsilon = 0$ and (b) $\epsilon = \frac{1}{2}$.

a diagnostic tool. If the system is integrable a pathline appears as a smooth solid curve and if the system is non–integrable the dots become smeared.

In the majority of the runs presented here we have used approximately 600 points per period. As noted in Aref [13] as τ tends to zero (that is the switching becomes faster), this system reverts to the steady configuration with both features 'turned on', that is two *stokeslets* situated at $Y = 1 + \epsilon$ and $Y = 1 - \epsilon$. The streamfunctions corresponding to $\epsilon = 0$ and $\epsilon = \frac{1}{2}$

(a)

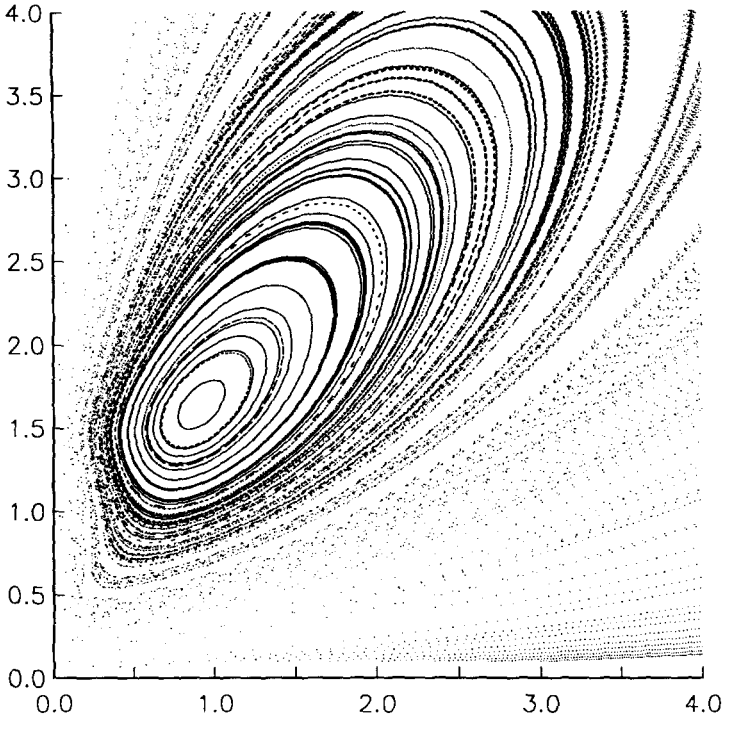

(b)

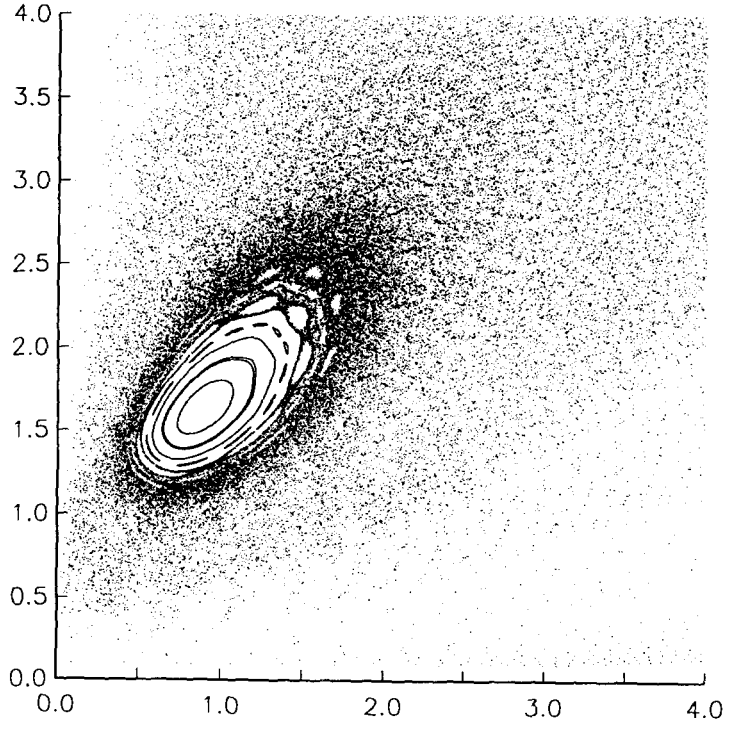

Fig. 7. Poincaré sections for (a) $\tau = 0.1$, (b) $\tau = 0.5$ and (c) $\tau = 1.0$.

(c)

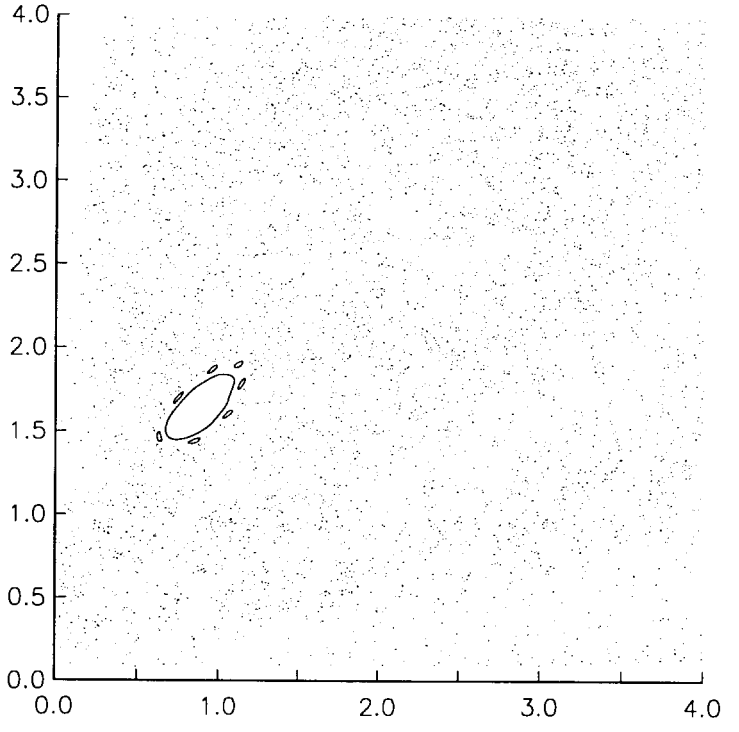

Fig. 7. contd.

(two steady *stokeslets*) are shown in Figs. 6(a) and 6(b) respectively. It is worth noticing that the stagnation point is higher in the second configuration, this is due to the fact that the higher *stokeslet* is effectively stronger. This can be seen by referring to the parameter α (that is the same value of α for a higher h corresponds to a greater F). We elect to discuss the case where $\epsilon = \frac{1}{2}$ similar results are obtained with other values of ϵ.

The Poincaré sections shown below correspond to 100 initial particles progressed through 2000 periods. In Fig. 7(a) we show a Poincaré section obtained by setting $\tau = 0.1$. It should be noted, as discussed in Aref that the majority of the region is integrable. This picture looks similar to the two *stokeslet* configuration depicted in Fig. 6(b). In Fig. 7(b) we show the effect of increasing τ to 0.5. There is still a central core region, however the majority of the flow is chaotic and hence will be well mixed and consequently filtered. Finally in Fig. 7(c) we show the case with $\tau = 1$, notice that there is still the inner region, however there does not appear to be any structure left outside this. (All that remains are the tiny islands which surround the main core of the eddy.) We appreciate that Fig. 7(c) represents ten times the physical time shown in 7(a), however, we believe 2000 periods is adequate for us to demonstrate the flow's characteristics. These calculations show that particle dispersion is significantly enhanced for larger values of τ but at a cost in that the process takes longer, which is a similar conclusion to that arrived at by Aref and Balachandar [14].

In order to further justify this assumption we include a set of 'stills' produced using $\tau = 0.1$ and $\tau = 1$. In each case 18 frames are shown and these correspond to the same physical time, that is frame 2 of Fig. 8(a) corresponds to the tenth period for $\tau = 0.1$ and frame 2 of Fig. 8(b) corresponds to the second period for $\tau = 1$. In both figures 10 concentric circles each containing 100 tracer particles are used and each frame shows $x, y \in (0,4)$. The 'blob' is

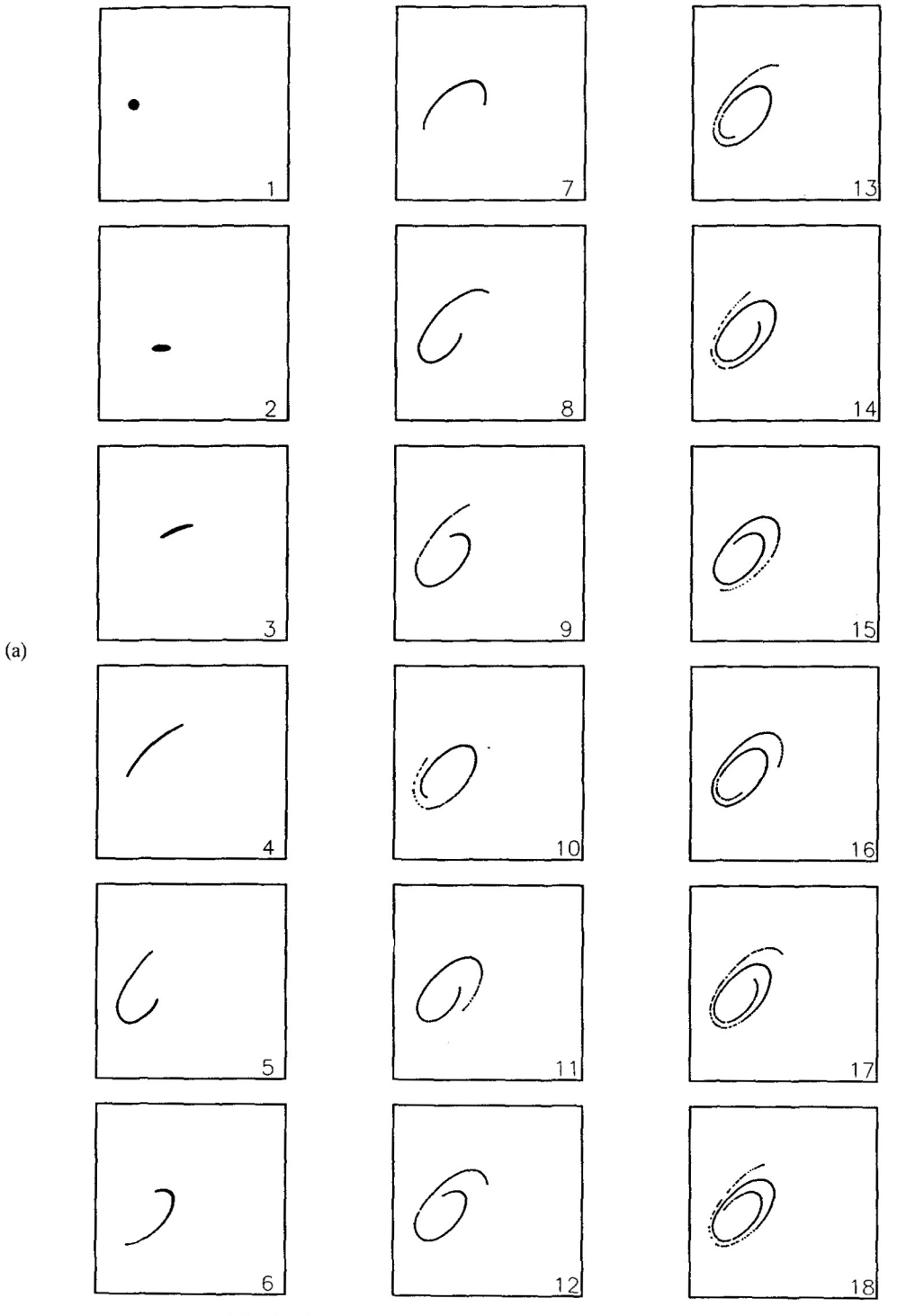

Fig. 8. The 'still' frames for (a) $\tau = 0.1$ and (b) $\tau = 1.0$.

(b)

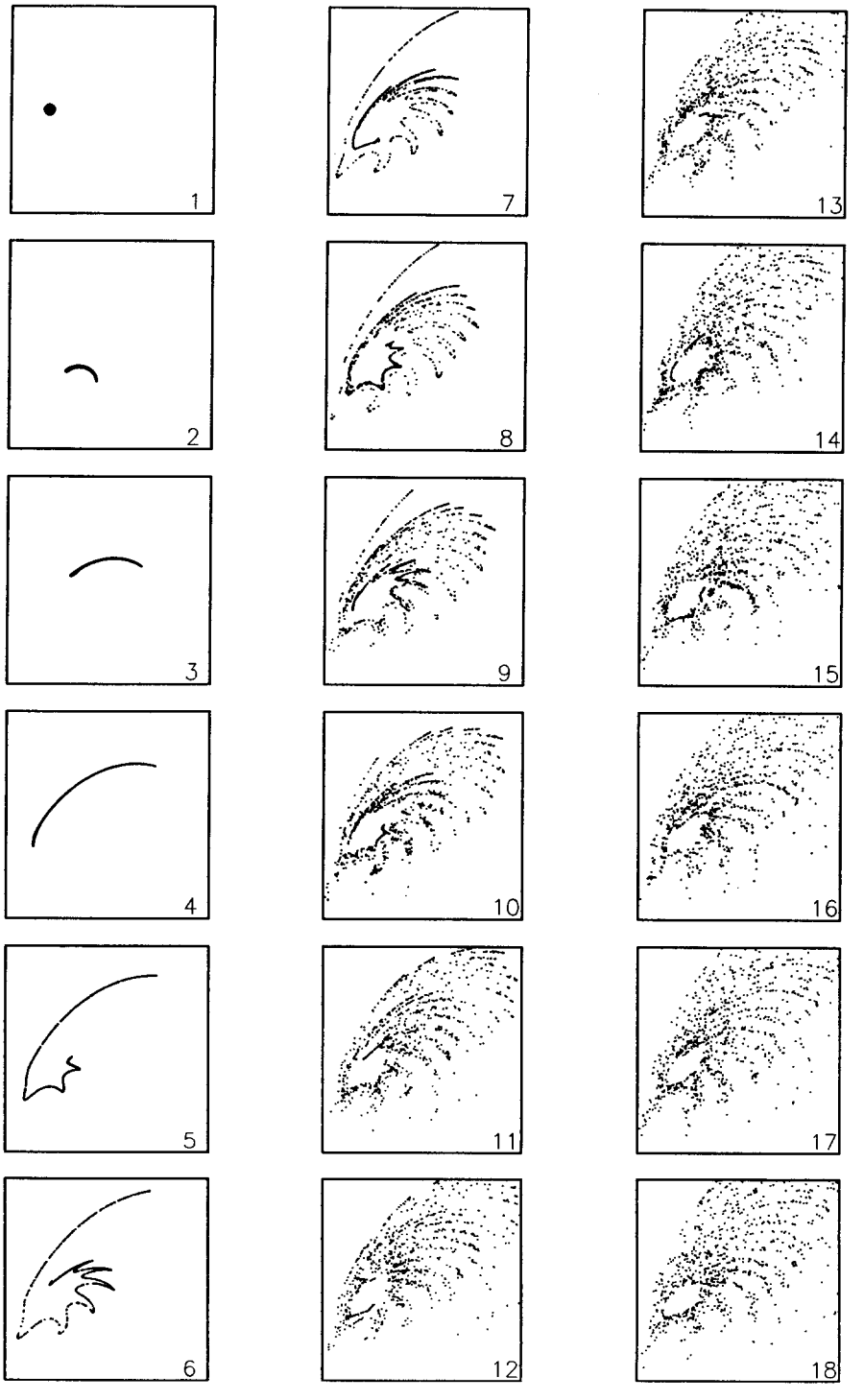

Fig. 8. contd.

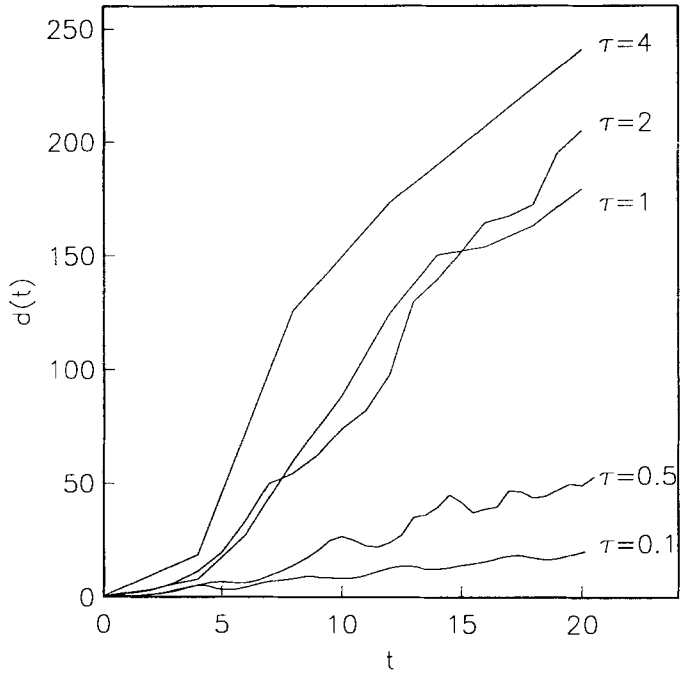

Fig. 9.

centred at $(\frac{3}{4}, 2)$ which is to the North-West of the core of the eddy (refer to 6(b)). The circles have radii from 0.01 to 0.1. This shows quite clearly the spreading, in that particles with similar starting positions can have very different ultimate positions in the chaotic case. In Fig. 8(a) we see the entrainment of the blob into the eddy, whereas in Fig. 8(b), although we can see slight entrainment, we note the severe spreading of the particles.

In a crude attempt to quantify this behaviour we have introduced a measure of the "boundary" of the tracer particles. If $\left(X_i^{(n)}, Y_i^{(n)}\right)$ are the particles originally situated on the outer circle, we define $d(t)$ as

$$d(t) = \sum_{i=2}^{N} \sqrt{\left(X_i^{(n)} - X_{i-1}^{(n)}\right)^2 + \left(Y_i^{(n)} - Y_{i-1}^{(n)}\right)^2}.$$

In Fig. 9 we plot $d(t)$ against physical dimensionless time for a variety of τ. This illustrates that the eventual disparity of the particles increases dramatically with τ, and hence will lead to better dispersion. Of course, since the system is chaotic and non-integrable, we cannot exploit the reversibility of Stokes flow to infer that this same approach would be valid for the reverse procedure of filtration, but nevertheless, it is 'food for thought'.

5. Conclusions

The material presented in this paper is based on the Green's function of the Stokes flow equations in the presence of a stationary no-slip boundary, an expression which can easily be derived from Lorentz's mirror image technique. The interpretation of the Green's function in terms of appropriate image singularities provides information on the far-field behaviour

of the fluid. The axisymmetric form of the equations shows a single closed toroidal eddy for the streamlines. The near and far-field behaviour is used to explain the fluid mechanics of ciliary propulsion while the toroidal character of the axisymmetric flow field is illustrated by consideration of the simpler two-dimensional twin eddy flow to postulate the concept of chaotic filtration. The calculations show that an initially 'compact' set of particles are dispersed widely (chaotically) for larger values of the period parameter τ. These ideas may be exploited by sessile organisms during feeding.

6. Acknowledgements

The authors wish to acknowledge, with thanks, the approval given by Professor M.A. Sleigh for allowing reproduction of Figs. 1(c) and (d) from his book [5] and for his interest in this work.

References

1. H.A. Lorentz, Eene algemeene stelling omtrent de beweging eener vloeistof met wrijving en eenige daaruit afgeleide gevolgen. *Zittingsverslag Koninkl. Akad. van Wetensch. Amsterdam*, 5 (1896) 168–175.
2. C.W. Oseen, *Hydrodynamik*. Leipzig: Teubner (1927) 337 pp.
3. J.R. Blake, A note on the image system for a *stokeslet* in a no-slip boundary. *Proc. Camb. Phil. Soc.* 70 (1971) 303–310.
4. J. Gray, *Ciliary Movement*. Cambridge: Cambridge University Press (1928) 162 pp.
5. M.A. Sleigh, *The Biology of Protozoa*. London, Edward Arnold (1973) 315 pp.
6. G.R. Fulford and J.R. Blake, Muco-ciliary transport in the lung. *J. Theor. Biol.* 121 (1986) 381–402.
7. J.R. Blake and A.T. Chwang, Fundamental singularities of viscous flow. Part I. The image systems in the vicinity of a stationary no-slip boundary. *J. Eng. Math.* 8 (1974) 23–29.
8. G.K. Batchelor, The stress system in a suspension of force free particles. *J. Fluid Mech.* 41 (1970) 545–570.
9. M.A. Sleigh and E. Aiello, The movement of water by cilia. *Acta Protozool.* 11 (1972) 265–77.
10. K. Aderogba and J.R. Blake, Action of a force near the planar surface between semi-infinite immiscible liquids at very low Reynolds numbers: Addendum. *Bull. Aust. Math. Soc.* 19 (1978) 309–318.
11. N. Liron and J.R. Blake, Existence of viscous eddies near boundaries. *J. Fluid Mech.* 107 (1981) 109–129.
12. J.J.L. Higdon, The generation of feeding currents by flagellar motions. *J. Fluid Mech.* 94 (1979) 305–330.
13. H. Aref, Stirring by chaotic advection. *J. Fluid Mech.* 143 (1984) 1–21.
14. H. Aref and S. Balachandar, Chaotic advection in a Stokes flow. *Phys. Fluids A* 29 (1986) 3515–3521.
15. J. De Frutos and J.M. Sanz-Serna, An easily implementable fourth-order method for the time integration of wave problems. *J. Comp. Phys.* 103 (1992) 160–168.